

Article

# Nanoscale Optical Trapping by Means of Dielectric Bowtie

Giuseppe Brunetti , Nicola Sasanelli, Mario Nicola Armenise and Caterina Ciminelli \* 

Optoelectronics Laboratory, Department of Electrical and Information Engineering, Polytechnic University of Bari, 70125 Bari, Italy; giuseppe.brunetti@poliba.it (G.B.); nicola.sasanelli@poliba.it (N.S.); marionicola.armenise@poliba.it (M.N.A.)

\* Correspondence: caterina.ciminelli@poliba.it

**Abstract:** Plasmonic and dielectric tweezers represent a common paradigm for an innovative and efficient optical trapping at the micro/nanoscale. Plasmonic configurations provide subwavelength mode confinement, resulting in very high optical forces, at the expense of a higher thermal effect, that could undermine the biological sample under test. On the contrary, dielectric configurations show limited optical forces values but overcome the thermal challenge. Achieving efficient optical trapping without affecting the sample temperature is still demanding. Here, we propose the design of a silicon (Si)-based dielectric nanobowtie dimer, made by two tip-to-tip triangle semiconductor elements. The combination of the conservation of the normal component of the electric displacement and the tangential component of the electric field, with a consequent large energy field confinement in the trapping site, ensures optical forces of about 27 fN with a power of 6 mW/ $\mu\text{m}^2$ . The trapping of a virus with a diameter of 100 nm is demonstrated with numerical simulations, calculating a stability  $S = 1$ , and a stiffness  $k = 0.33$  fN/nm, within a footprint of 0.96  $\mu\text{m}^2$ , preserving the temperature of the sample (temperature variation of 0.3 K).

**Keywords:** optical nanocavity; dielectric bowtie; nanoparticle optical trapping



**Citation:** Brunetti, G.; Sasanelli, N.; Armenise, M.N.; Ciminelli, C. Nanoscale Optical Trapping by Means of Dielectric Bowtie. *Photonics* **2022**, *9*, 425. <https://doi.org/10.3390/photonics9060425>

Received: 18 May 2022

Accepted: 14 June 2022

Published: 16 June 2022

**Publisher's Note:** MDPI stays neutral with regard to jurisdictional claims in published maps and institutional affiliations.



**Copyright:** © 2022 by the authors. Licensee MDPI, Basel, Switzerland. This article is an open access article distributed under the terms and conditions of the Creative Commons Attribution (CC BY) license (<https://creativecommons.org/licenses/by/4.0/>).

## 1. Introduction

Trapping techniques use engineered forces to accurately control and manipulate objects in mesoscopic systems with length scales from tens of nanometers to hundreds of micrometers [1,2]. The understanding of the light interaction with the matter at a micro/nanometer scale paves the way to improve the knowledge of the properties of materials and the use of trapping in interesting application fields, such as sensing [3] and quantum systems [4]. In particular, the main capabilities of the trapping techniques have been exploited in the natural sciences fields, primarily in support of modern medicine, i.e., for monitoring inter- and intracellular processes or the manipulation of viruses and bacteria [5].

Since Ashkin's pioneering research [6,7], optical trapping configurations have been developed to trap small cells and bacteria [8], first preventing the contact of the target with the device and then damaging or disrupting the target object, as required in non-invasive medicine. Conventional optical trapping techniques exploit the forces exerted on the target by focused laser beams [9]. However, although bulk tweezers with focal lenses that provide an effective trapping of micro-sized particles are largely used, this approach suffers from low optical gradient force, due to the diffraction limit, and trapping situ larger than the particle itself. To overcome these challenges, the development of efficient trapping devices remains a hot research topic [10].

An optical approach ensures a high trapping efficiency and the stability of the target object in the trapping situ. During recent decades, several configurations of photonic devices, mainly based on photonic resonant devices [8] such as photonic crystals [11,12] and ring resonators [13,14], plasmonic devices [15], or hybrid configurations [16,17], have been demonstrated. Photonic resonant devices have been proposed as optical tweezers,

to exploit their high spectral and spatial energy confinement, which strongly depends on the high  $Q$ -factors and low mode volume. The trapping of a single protein using a power of 10 mW has been experimentally demonstrated in [18] by using a 1D PhC cavity, with a stiffness  $k$  in the order of hundredths of fN/( $\mu\text{m}/\text{mW}$ ). Nevertheless, a stable trapping of polystyrene particles with diameters of 500 nm and 200 nm has been demonstrated with a silicon-based ring resonator [13] and microdonuts [19], respectively, with optical power in the order of microwatts. The short trapping time represents the main bottleneck of photonic resonant optical tweezers, mainly caused by the optical gradient force not being sufficient to trap the target for a “long” time. To mitigate this issue, engineered photonic resonant configurations, as metasurfaces, have also been proposed in the literature, to ensure an efficient trap of thousands of objects, with a power value density less than tens  $\mu\text{W}/\text{site}$  and optical forces of tens of fN, at the expense of a larger footprint and higher complexity [20]. To overcome such issues, plasmonic antenna systems have been proposed, aiming to control light at the nanometer scale with a large electromagnetic field within deep subwavelength volumes [15]. The plasmonic enhancement is strictly correlated with the near- and far-field properties of metallic nanostructures that confine the light within small volumes and amplify the intensity of optical fields by orders of magnitude, so that they are useful in surface-plasmon-sensing applications [21]. The trapping of particles with diameters of tens of nm has been experimentally demonstrated by using different plasmonic configuration, such as coaxial apertures [22], single/double nanoholes [23,24], and bowties [25], with very low optical power values ( $\approx\text{mW}$ ) and stiffness of hundreds of fN/(nm/mW). However, the critical challenge of the plasmonic trapping configurations is related to the thermal effect, due to the Joule effect caused by the strong absorption loss of the metal layers at high operating frequencies, which could lead to thermophoresis or the boiling of the fluid surrounding the particles [26]. These effects could irreversibly undermine the biological sample and then affect the robustness of the measurements. Countermeasures have been proposed to mitigate similar behavior, such as integrating a high thermal conductive heat sink with the plasmonic nanoantenna [27] or exploiting the heat sink behavior of the metallic film itself [28]. However, even when using these techniques, the temperature surrounding the sample is still high (in the order of a few K). This challenge led to the development of dielectric nanoantennas, preventing the thermal effects with simple configurations and high stiffness [29–32]. The high electric field confinement of dielectric antennas is ensured by their strong electric and magnetic resonant modes, known as “hotspots”. Worsening temperatures, correlated with strong electric field confinement, are prevented by using high thermal conductive materials such as silicon. In this context, the efficient optical trapping of 20 nm and 100 nm polystyrene nanosphere has been demonstrated by using two silicon pillars within a ring resonator, with a stiffness of about 0.01 fN/(nm/mW) and an optical power of about 10 mW [29]. Recently, dielectric bowtie nanocavities have been also theoretically investigated [30,31], demonstrating a deep subwavelength mode volume and high  $Q$ -factor, with a relatively high Purcell factor. Although these devices have been proposed for several applications, such as a high-efficiency single photon source, threshold-less nanolasers, and cavity QED strong coupling experiments, the capability of this device as an optical tweezer has not yet been proved, to our knowledge [30,31].

Here, we propose the investigation of a nanocavity made by silicon tip-to-tip triangles acting as optical tweezers for trapping beads with a diameter of 100 nm, as the common *Coronaviridae* or *Paramyxoviridae* virus family. The energy field confinement within the trapping site has been maximized by engineering the wedges and then tailoring the “slot” and “antislot” effect, as described in the next few sections. The improvement of the energy confinement within the trapping volume preserves the efficiency of the trapping with regard to any manufacturing/setup issues, making the proposed device robust with repeatable performances. A force along the normal axis of 27.45 fN, with stiffness of about 0.33 fN/nm, has been calculated for the trapping of a 100 nm bead with an input power of 5.77 mW and a temperature change of 0.3 K that correspond to a trapping stability  $S = 1$ ,

ensuring a stable trapping for several seconds, as stated in [29]. All these features, combined with the robustness of fabrication, make the proposed device suitable for multifunctional applications based on light–matter interactions, including enhanced spectroscopy, SERS, fluorescence, and biosensing.

## 2. Dielectric Bowtie

The proposed device consists of a three-dimensional dielectric nanocavity, including two tip-to-tip semiconductor wedges (*TTSWs*), forming the so-called nanobowtie dimer shown in Figure 1, realized in Silicon-On-Insulator (*SOI*) technology. The *TTSWs* have the same physical and geometrical features, with an out-of-plane light excitation along the *z*-axis. In particular, the silicon-based dimers show a thickness *t* equal to 220 nm, placed on top of a silica dioxide ( $\text{SiO}_2$ ) layer. The *TTSWs* show a wedge shape, with a height *h* and a wedge tip angle  $\alpha$ .

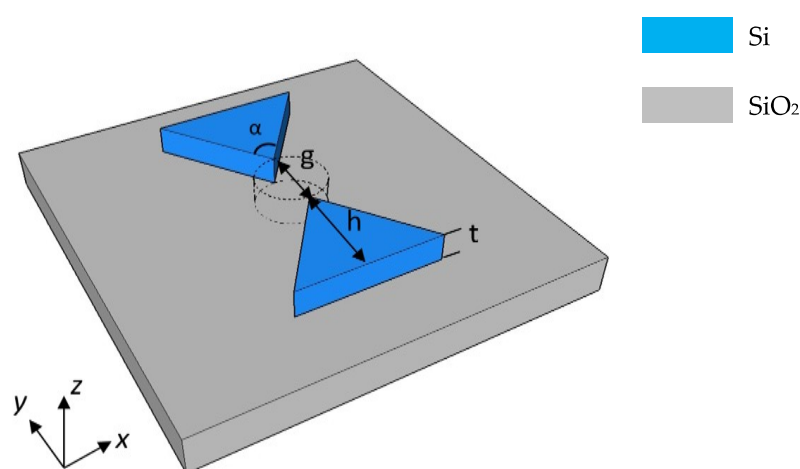


**Figure 1.** Schematic of the investigated nanobowtie dimer configuration in *SOI* platform (*t*: silicon thickness; *g*: width of the trapping site, sketched with a dotted cylinder;  $\alpha$ : wedge angle; *h*: wedge height).

The wedges are symmetrically placed with respect to the center of the trapping site, sketched with a dotted cylinder with a diameter equal to *g*, and spatially separated by *g*. The proposed configuration is surrounded by water ( $\text{H}_2\text{O}$ ), used to transport biological species. Although small wavelengths are preferred in order to enhance the trapping efficiency by reducing the scattering force [33], this benefit is mitigated by a gradient force proportional to the operating wavelength and by a strong field confinement within the trapping region, in nanoscale, in a large spectrum region. Moreover, the low cost and easy availability of the light sources at telecommunication wavelengths paves the way to their use in several applications, including optical trapping [34]. Therefore, an operating wavelength  $\lambda_0$  equal to 1550 nm is assumed, as in [34]. The relative refractive indexes of Si,  $\text{SiO}_2$ , and water, at 1550 nm, are  $n_{\text{Si}} = 3.48$ ,  $n_{\text{SiO}_2} = 1.444$ , and  $n_{\text{H}_2\text{O}} = 1.318 + 9.86 \times 10^{-5} i$ , respectively [35–37].

The electromagnetic behavior of the proposed configuration results from the exploitation of the first Boundary Condition (BC), which requires the continuity of the normal component of the electric field displacement. It ensures that the maximum of the electromagnetic energy density is confined to the low-permittivity region (slot effect) that is greatly increased with respect to the maximum energy density in a high-permittivity material, such as the *TTSWs*. The slot effect ensures the squeezing of the mode along *y* and *x* axes in the dielectric gap, resulting in a large electric field discontinuity at the high-index contrast interfaces, with a consequent light enhancement and confinement, and the electric field enhancement (“hotspot”) in proximity of the wedge tip of each *TTSWs* [38,39].

Therefore, the *TTSWs* function as capacitors, with the energy stored in the low-permittivity region (dotted cylinder in Figure 1).

### 3. Design to Enhance the Energy within the Trapping Site

The proposed configuration is designed to maximize the electromagnetic energy confined in the trapping site. The most common approach to designing optical nanocavities aims to minimize the effective area of the mode in the trapping region [15,16,30,31], expressed as the ratio between the integral of the electromagnetic energy density and its maximum. However, this approach neglects the amount of energy confined in the trapping site, confining the mode in a small volume and then becoming very sensitive to manufacturing issues. Therefore, we have introduced a new figure of merit, EC, representing the energy confinement in the trapping site, expressed as the ratio between the integral of the electromagnetic energy density in the trapping site and the integral of the electromagnetic energy density in the whole volume surrounding the nanoantenna:

$$EC = \frac{\int \int \int_{\text{trapping site}} W(\mathbf{r}) d^3\mathbf{r}}{\int \int \int_{\text{volume}} W(\mathbf{r}) d^3\mathbf{r}} \quad (1)$$

where  $W(\mathbf{r})$  is the electromagnetic energy density ( $W(\mathbf{r}) = \frac{1}{2}[\epsilon(\mathbf{r})|E(\mathbf{r})|^2 + \mu(\mathbf{r})|H(\mathbf{r})|^2]$ ) and  $\mathbf{r} = x \mathbf{a}_x + y \mathbf{a}_y + z \mathbf{a}_z$ . This figure of merit responds to the need of a high energy confinement within the trapping to ensure a powerful trapping even with a small mode volume.

As previously reported, the trapping site is considered a fictitious cylinder with a thickness  $t$  and a diameter  $g$ . Since the target molecule to be trapped shows a diameter of about 100 nm, such as the RNA-based *Coronaviridae* or *Paramyxoviridae* virus families [40,41], a gap  $g$  of 120 nm is suggested, based on a conservative approach, to ensure the fabrication robustness by avoiding the particle sticking at the tips. A 3D Finite Element Method (FEM) approach is used to simulate the electromagnetic behavior of the investigated configurations. In particular, the device is designed to define the best configuration in terms of  $\alpha$  and  $h$ . The 3D mapping of the normalized figure-of-merit  $EC_{\text{norm}}$  is shown in Figure 2a, with an impinging optical power  $P_{\text{norm}} = 1 \text{ mW}/\mu\text{m}^2$  polarized along the  $y$ -direction. The inconstant behavior of the electric energy confinement in the trapping site is due to the spreading of the electromagnetic energy in the in-plane cladding layers, for configurations with  $h < 260 \text{ nm}$  and  $\alpha < 110^\circ$ , or in the silicon wedges, for configurations with  $h > 260 \text{ nm}$  and  $\alpha > 110^\circ$ , due to the additional high-permittivity antislot effect. In the remaining regions, the electromagnetic field moves from high to low, or vice versa, in the permittivity region.

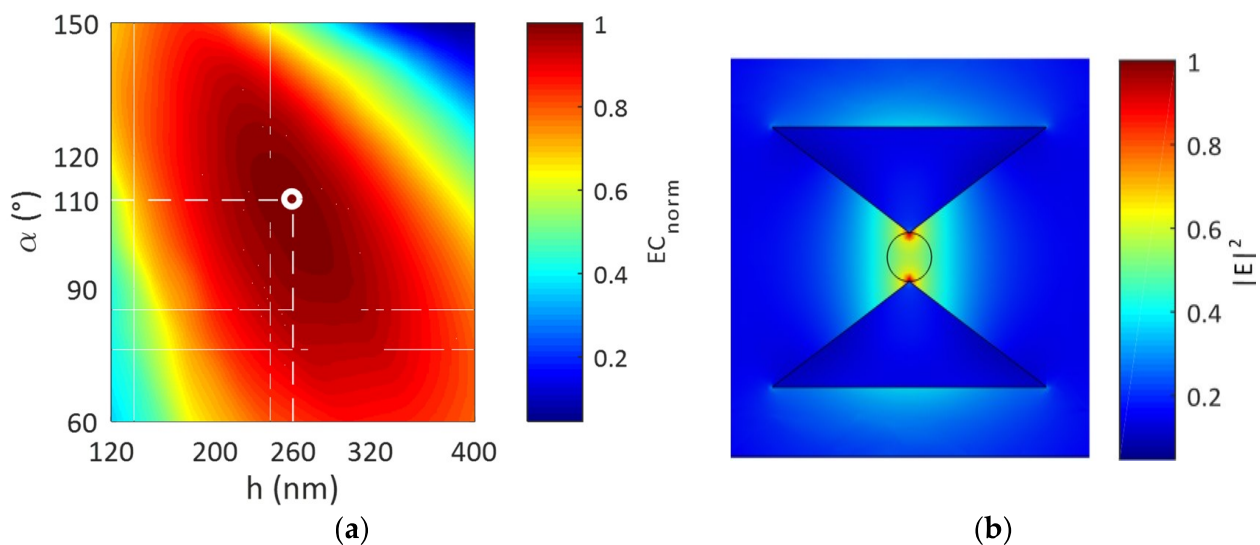


**Figure 2.** (a) 3D representation of  $EC_{\text{norm}}$ , by considering  $P_{\text{norm}} = 1 \text{ mW}/\mu\text{m}^2$ ; (b) electric field distribution for the proposed dielectric bowtie with  $t = 220 \text{ nm}$ ,  $\alpha = 110^\circ$ ,  $h = 260 \text{ nm}$ , and  $g = 120 \text{ nm}$ .

This effect is related to the fulfillment of the second boundary condition that requires the continuity condition of the tangential electric field between two different materials. Therefore, this effect spreads the electric field in the trapping site with a consequent decrease in the electric field confined in the trapping region.

The configuration with  $\alpha = 110^\circ$  and  $h = 260$  nm shows the highest normalized EC, expressed as  $EC_{norm}$ , (white empty circle in Figure 2a), as shown by Figure 2b, with a resulting total footprint  $A$  of about  $0.96 \mu\text{m}^2$ . The major component of the electric field is along the y-direction, representative of the quasi-TE polarized mode in the nanocavity. The electromagnetic energy density is mainly confined within the gap region, without spread in the cladding or dielectric material, typical of the slot effect, ensuring a stable trapping of the target particle.

In order to demonstrate the overcoming of the heating problems related to plasmonic nanoantennas, numerical simulations on the temperature behavior were carried out. The top view of the steady-state temperature distribution for the investigated configuration is reported in Figure 3a by considering an input optical power of  $1 \text{ mW}/\mu\text{m}^2$ . The temperature rises in correspondence with the trapping site, where the electromagnetic density is highly confined, as expected, with a maximum temperature increase  $\Delta T$  of 0.07 K. Moreover, the  $\Delta T$  change created by varying the input optical power  $P_{norm}$ , and then the total optical power  $P_{tot}$  ( $=P_{norm} \times A$ ) has been calculated (see Figure 3b), measuring a slope of  $7.51 \times 10^{-2} \text{ K}/(\text{mW}/\mu\text{m}^2)$ . Similar values confirm the suitability of the dielectric nanoantennas for biological species trapping, because of the negligible temperature increase in contrast with the plasmonic nanoantennas where an increase in temperature of about 100 K has been obtained in [29], caused by the thermophoresis effect. The small temperature growth also preserves the vitality of the trapped biological species.

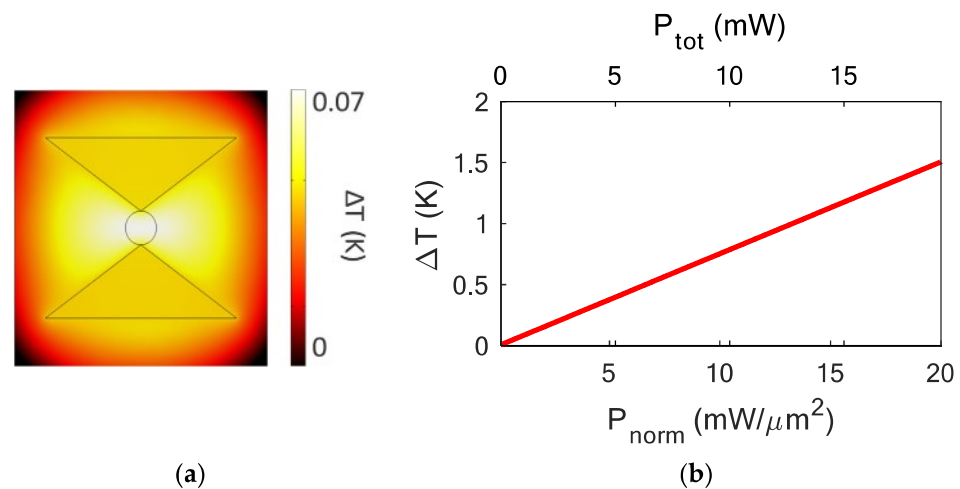


**Figure 3.** (a) Top view of the temperature distribution  $\Delta T$  (K) ( $\Delta T = T - T_0$ ,  $T_0 = 293.15$  K) for the designed configuration at  $z = 110$  nm, with  $P_{norm} = 1 \text{ mW}/\mu\text{m}^2$ ; (b) temperature increase  $\Delta T$  in the trapping region as a function of the normalized input optical power  $P_{norm}$  and then  $P_{tot}$  ( $A = 0.96 \mu\text{m}^2$ ).

#### 4. Numerical Results on the Optical Trapping and Discussions

Three-dimensional *FEM* simulations with the Maxwell Stress Tensor (*MST*) approach have been used to calculate the optical forces exerted by the proposed nanocavity on a spherical particle with a diameter  $d$  of 100 nm and a refractive index equal to 1.50, representative of some viruses, i.e., *Influenza A* [42,43] and *HIV-1* [44]. The software COMSOL Multiphysics® has been used for e.m. and thermal simulations by combining the heat transfer and optical physics. According to the method described in [45], we have evaluated the optical force as the surface integral, on a surface with a radius few nm larger than the particle radius, of the vectorial product of the Maxwell stress tensor and the outgoing vector normal to the surface.

In particular, the optical forces have been evaluated on the particle under test in different positions along the  $x$ ,  $y$ , and  $z$  axes. The positions  $x = 0$ ,  $y = 0$ , and  $z = 0$  correspond to the central point of the trapping site at the Si-SiO<sub>2</sub> interface (see Figure 4). In order to estimate the trapping efficiency of the designed structures, the optical forces  $F_i$  ( $i = x, y, z$ ) on the target bead have been calculated by varying the position of the bead, as shown in Figure 5.

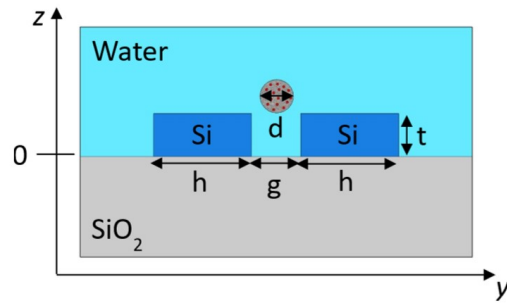


Figure 4. Lateral view of the nanocavity ( $z$ - $y$  directions) with a trapped particle ( $d = 100$  nm).

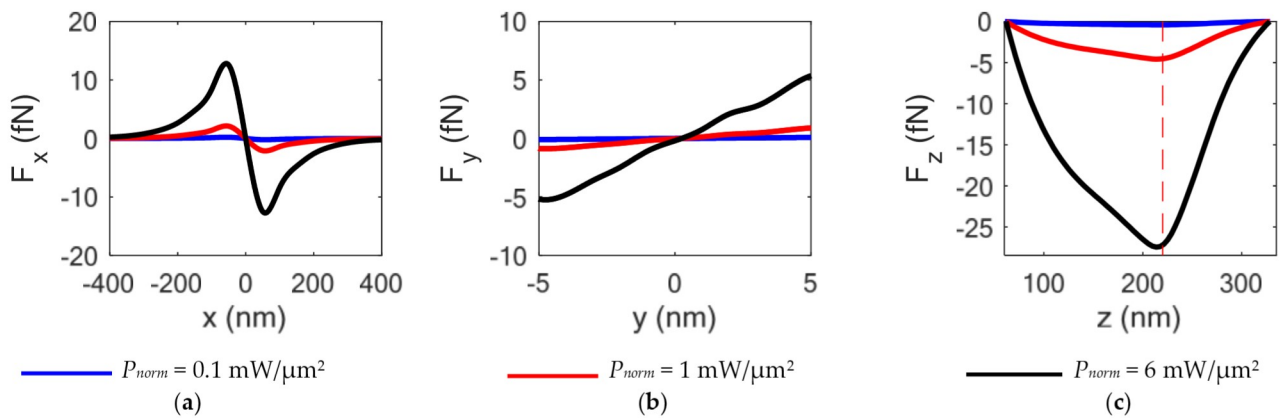
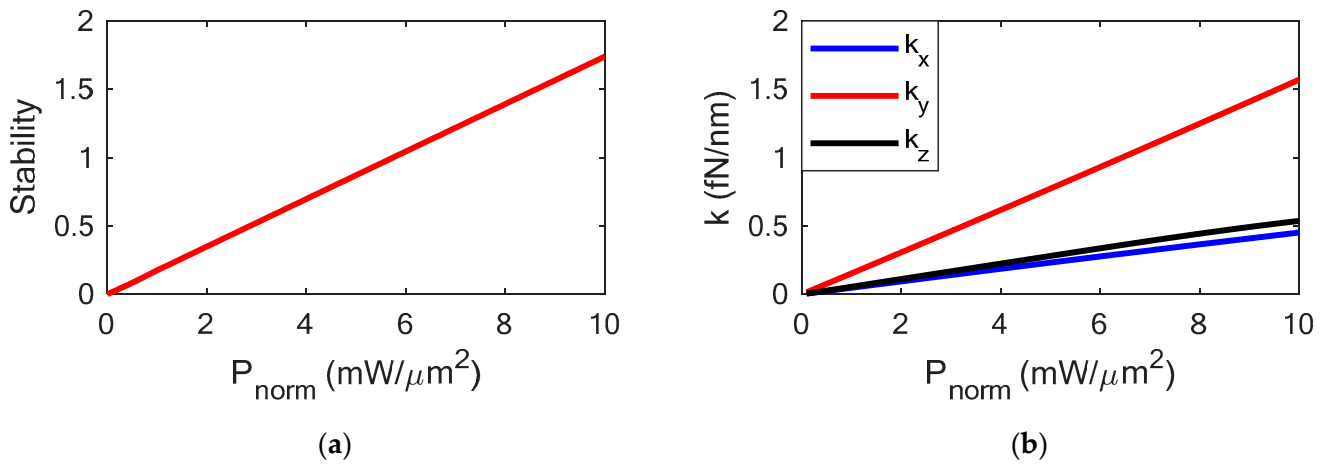


Figure 5. Optical forces  $F_x$ ,  $F_y$ , and  $F_z$ , varying the input power  $P_{norm}$  and considering a particle with  $d = 100$  nm.

With the bead placed at  $(x = 0, y = 0)$ ,  $F_z$  was calculated, observing a linear increase in the optical forces by varying the input power with a peak at  $z = z_{eq} = 213.5$  nm, close to the top surface of the bowtie.  $z_{eq}$  is the  $z$ -coordinate of the equilibrium point, where the field gradients are the largest ones. Optical forces  $F_x$  and  $F_y$  were calculated by varying the bead position in both axes at  $z = z_{eq}$ . In particular, both forces show symmetry with respect to the position  $x = x_{eq} = 0$  and  $y = y_{eq} = 0$ , that represent the  $x$ - and  $y$ -coordinate of the equilibrium point. Along the  $y$ -direction, the movement of the bead is limited by the gap  $g$ , while along the  $x$ -direction, the bead undergoes the optical forces from  $x = -58$  nm to  $x = +58$  nm. For outer values, the bead can be considered free to move. An efficient and stable trapping requires the optical forces to be larger than the repulsive thermal force that could push the particle away from the equilibrium point. The stability of the nanocavity has been estimated as  $S = U / (k_B \cdot T_c)$ , where  $U$  is the potential energy that corresponds to the work required to bring the nanoparticle from a free position to the trapping site [J],  $k_B$  is the Boltzmann constant [J/K], and  $T_c$  is the temperature in Kelvin [K], also taking into account the temperature rise due to the trapping effect [16]. The stability is usually referred to as the potential depth [46]. An increase in the stability corresponds to a longer trapping time, according to the Kramers theory [47,48]. In particular, the trapping time  $t_{trap}$  is expressed as  $t_{trap} \propto \exp(U / k_B T)$ . Therefore, the potential energy should be greater than or equal to  $k_B T$ . Stability values larger than 1 are required to ensure the dominance of the optical forces with respect to the thermal one, in order to increase the trapping time. A trapping time of several seconds has been observed with other dielectric nanotweezers of  $S \sim 1$  [29]. Larger  $S$  values lead to a longer trapping time.

Figure 6a shows the stability of the proposed configuration as a function of the normalized input power. A stability of about 1.2 (potential energy of 1.2  $k_B T$ ) has been calculated with an input optical power  $P_{norm}$  of 6  $mW/\mu m^2$  ( $P_{tot} = 5.77 mW$ ), where  $F_z$  shows a peak of 27.45 fN. This performance demonstrates the high stability of a nanoparticle in the trapping site, which corresponds to a long trapping time (tens of seconds), with low input power. However, the experimental demonstration of optical trapping could introduce several physical factors that affect the optical trapping time. In particular, the pointing stability and the power fluctuations of the laser, the resolution of the motion stages, and the environment, in terms of temperature changes, acoustic noise, and mechanical vibrations, are crucial factors for the success of experimental trapping [9].



**Figure 6.** Stability (a) and stiffness  $k$  (b) of the trapping event by varying the input optical power  $P_{norm}$ .

To evaluate the trapping stability, the trapping stiffness  $k_i$ , expressed as  $k_i = \partial F_i / \partial i$  ( $i = x, y, z$ ), has been evaluated (Figure 6b) at the equilibrium point. A high stiffness value ensures a stable position of the particle under test at the equilibrium point. For  $P_{norm} = 6 mW/\mu m^2$ ,  $k_x = 0.27 fN/nm$ ,  $k_y = 0.93 fN/nm$ , and  $k_z = 0.33 fN/nm$  have been calculated. The strong electric field confinement along the y-axis leads to the higher value of stiffness.

In order to further demonstrate the trapping capability of the designed device, the optical forces have been mapped in the whole device area (Figure 7). A value of  $z$  equal to 275 nm was assumed to ensure the movement of the bead in the x-y plane.

As revealed by the distribution of the force module (Figure 7d), the slot effect allows the stable trapping of the target particle only in the desired trapping region where the force peak is significant. The symmetrical distribution of the forces  $F_x$  and  $F_y$  with respect to  $x = 0$  and  $y = 0$ , respectively, allows the particle to place itself in the trapping site. Although a direct comparison between the different trapping techniques is difficult due to the dependence of the performance on the particle size, the proposed device shows a stiffness (0.0572 pN/nm/W) significantly higher than other dielectric cavities for trapping (e.g., Z. Xu et al. report 0.0027 pN/nm/W for the trapping of 20 nm bead [29]), with a significant saving in terms of power (e.g., H. J. Yang et al. report a power of 250 mW for a stable trapping ( $S = 10$ ) of 75 nm bead [49]) and footprint, with respect to the resonant cavities [11], also preserving the sample temperature, in contrast with the plasmonic nanocavities [50].

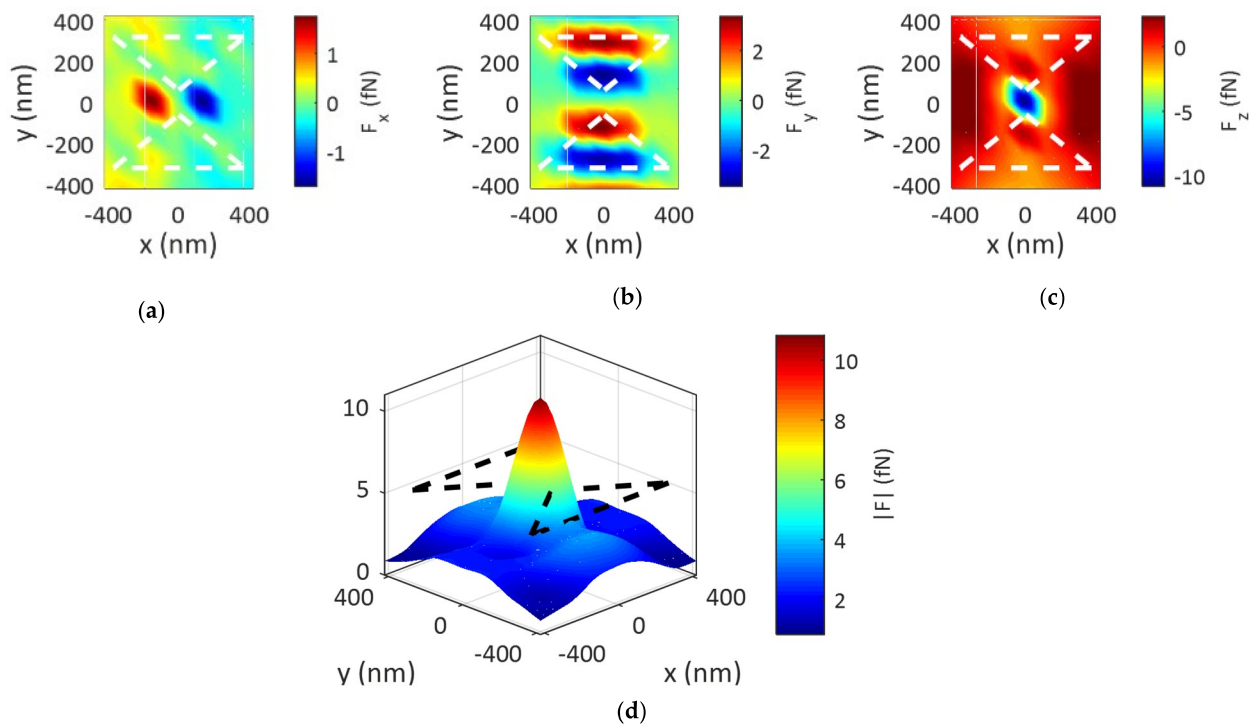


**Figure 7.**  $F_x$  (a),  $F_y$  (b),  $F_z$  (c), and  $|F|$  (d) distribution within x-y plane with  $P_{norm} = 6 \text{ mW}/\mu\text{m}^2$  and  $z = 275 \text{ nm}$ .

Finally, the robustness of the proposed device with regard to issues on the testing setup, i.e., polarization or operating wavelength change, and fabrication technique, has been investigated. Figure 8a shows the trend of the optical force  $F_z$  at the equilibrium point by varying the polarization direction of the input beam, represented as the angle  $\gamma$  between the y-axis and the beam. As expected, the optical forces became negligible for  $\gamma = 45^\circ$  and the bead is repelled from the trapping site for  $\gamma > 45^\circ$ . The second-order shape of the  $F_z$  vs.  $\gamma$  trend makes the proposed device very robust with respect to the polarization direction: a change in the optical force of less than 10% has been calculated for  $\gamma$ , ranging from  $0^\circ$  to  $15^\circ$ .

Moreover, the effect of the operating wavelength on the performance was explored by taking into account the material dispersion in terms of refractive index and absorption losses. The trend of the optical forces  $F_z$  vs. operating wavelength  $\lambda_0$  is shown in Figure 8b. For  $\lambda_0 < 1300 \text{ nm}$ , the antislot effect arises. As expected, according to the Rayleigh theory [33], the optical forces increase as the operating wavelength decreases due to the mitigation of the scattering effect. However, although a change in the scattering force of more than 80% is expected within the range 1300–1700 nm, since the scattering force is directly proportional to  $(1/\lambda_0)^4$ , the force gradient attenuates the wavelength dependence.

In fact, an optical force  $F_z$  change of  $\pm 7\%$  over a range of 400 nm, with respect to  $\lambda_0 = 1550 \text{ nm}$ , has been obtained, with a resulting negligible stability change of about  $\pm 0.23$ . At the same time, this result demonstrates an attenuation of the force dependence by the wavelength and a very high robustness of the device to  $\lambda_0$ .

In order to take into account the manufacturing issues that could lead to the rounding of the wedges, the effect of a fillet shape of the wedges has been investigated (see the inset of Figure 8c). According to the literature [51], a maximum value of the radius  $R = 20 \text{ nm}$  has been set. As the radius increases, together with the gap  $g$ , the optical forces decrease, with a maximum change in the force of 5%, which leads to a stability change of 0.16. This behavior is justified by designing the device to improve the mode confinement with a volume region, confirming the strength of the proposed structures to any fabrication issue, in contrast to the behavior of plasmonic tweezers [16].

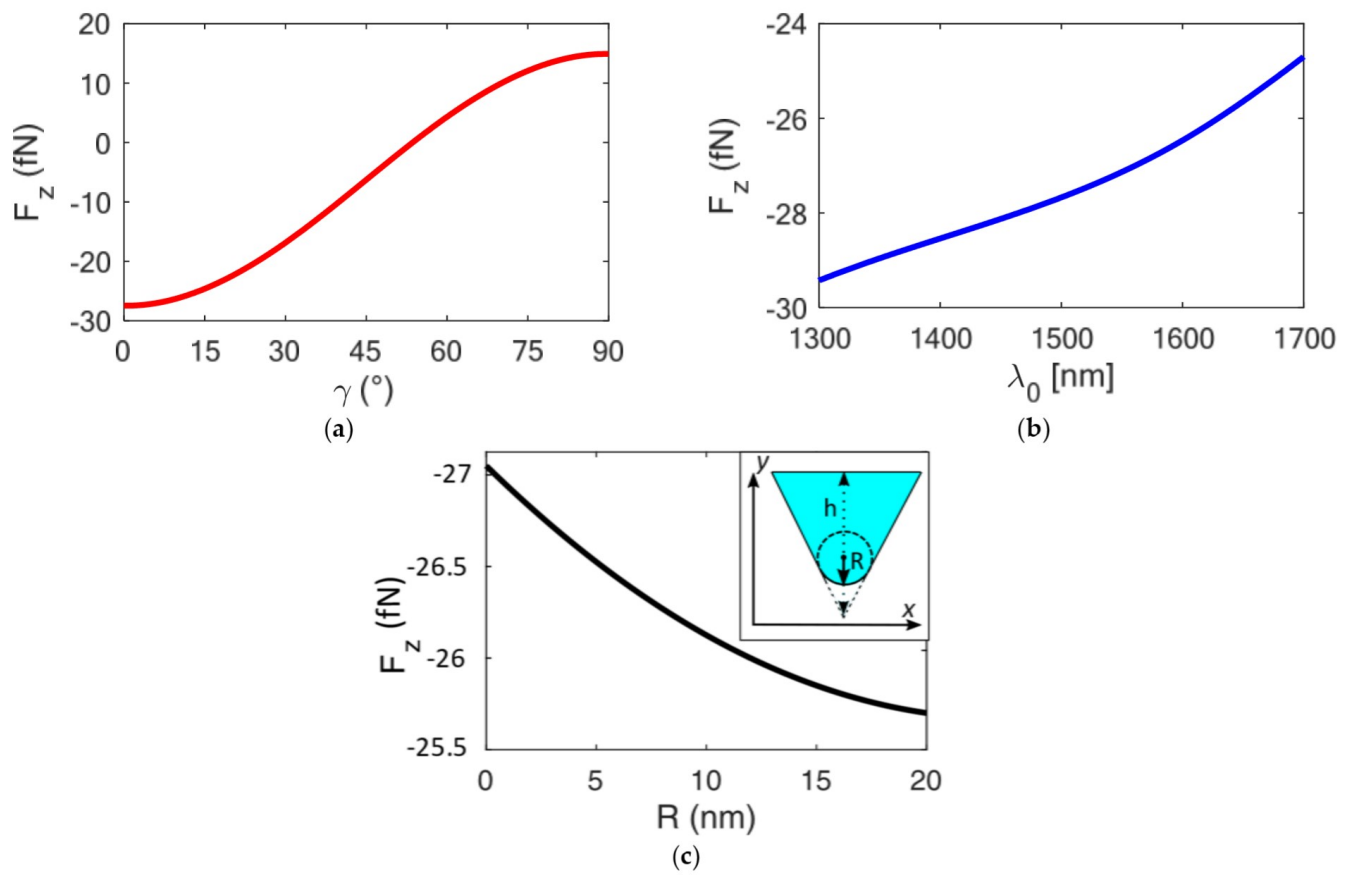


**Figure 8.** Optical force  $F_z$  behavior at the equilibrium point, varying the polarization direction  $\gamma$  (a), operating wavelength  $\lambda_0$  (b), and the radius  $R$  of the wedge fillet shape (c) with  $P_{norm} = 6 \text{ mW}/\mu\text{m}^2$ .

**5. Conclusions**

The design of efficient devices for trapping and manipulation of the biological species is needed to support classical medicine. Here, we have investigated a nanocavity, based on silicon wedges, useful as trapping device for virus with a size in the order of hundreds of nm. The design of the proposed configurations has been carried out by using 3D FEM simulations, aiming at maximizing the electromagnetic field density in the trapping site. An optical force of 27.45 fN, with a stability of more than 1 and a stiffness  $> 0.3 \text{ fN/nm}$ , has been demonstrated for a trapping of 100 nm bead, as for *Influenza A* or *HIV-1* virus, also minimizing the thermal heating effect ( $\Delta T \approx 0.3 \text{ K}$ ). The proposed device shows a notable improvement in the stiffness value with respect to other dielectric tweezers reported in the literature, with a significant saving of the working power in comparison with plasmonic tweezers. The results confirm the suitability of the proposed dielectric device for trapping a single nanoparticle (with a diameter of 100 nm) with very high stability and a long trapping time (in the order of tens of seconds).

**Author Contributions:** Conceptualization, G.B. and C.C.; methodology, G.B., M.N.A. and C.C.; software, G.B. and N.S.; investigation, N.S.; resources, G.B. and C.C.; writing—original draft preparation, G.B.; writing—review and editing, N.S., M.N.A. and C.C.; supervision, C.C. All authors have read and agreed to the published version of the manuscript.

**Funding:** This research was funded by POR Puglia FESR FSR 2014–2020–Action 10.4–“Research for Innovation” (REFIN) Initiative.

**Data Availability Statement:** Not applicable.

**Conflicts of Interest:** The authors declare no conflict of interest.

## References

1. Kirchain, R.; Kimerling, L. A roadmap for nanophotonics. *Nat. Phot.* **2007**, *1*, 303–305. [[CrossRef](#)]
2. Grier, D.G. A revolution in optical manipulation. *Nature* **2003**, *424*, 810–816. [[CrossRef](#)] [[PubMed](#)]
3. Choi, M.S.; Lee, G.H.; Yu, Y.J.; Lee, D.Y.; Lee, S.H.; Kim, P.; Hone, J.; Yoo, W.J. Controlled charge trapping by molybdenum disulphide and graphene in ultrathin heterostructured memory devices. *Nat. Comm.* **2013**, *4*, 1624. [[CrossRef](#)] [[PubMed](#)]
4. Hohenester, U. *Nano and Quantum Optics: An Introduction to Basic Principles and Theory*; Springer: Cham, Switzerland, 2020.
5. Ashkin, A.; Dziedzic, J.M. Optical trapping and manipulation of viruses and bacteria. *Science* **1987**, *235*, 1517–1520. [[CrossRef](#)] [[PubMed](#)]
6. Ashkin, A. Acceleration and trapping of particles by radiation pressure. *Phys. Rev. Lett.* **1970**, *24*, 56. [[CrossRef](#)]
7. Ashkin, A.; Dziedzic, J.M.; Bjorkholm, J.E.; Chu, S. Observation of a single-beam gradient force optical trap for dielectric particles. *Opt. Lett.* **1986**, *11*, 288–290. [[CrossRef](#)]
8. Conteduca, D.; Dell’Olio, F.; Krauss, T.F.; Ciminelli, C. Photonic and plasmonic nanotweezing of nano-and microscale particles. *Appl. Spectr.* **2017**, *71*, 367–390. [[CrossRef](#)]
9. Neuman, K.C.; Block, S.M. Optical trapping. *Rev. Sci. Instrum.* **2004**, *75*, 2787–2809. [[CrossRef](#)]
10. Maragò, O.M.; Jones, P.H.; Gucciarini, P.G.; Volpe, G.; Ferrari, A.C. Optical trapping and manipulation of nanostructures. *Nat. Nanotech.* **2013**, *8*, 807. [[CrossRef](#)]
11. Mandal, S.; Serey, X.; Erickson, D. Nanomanipulation using silicon photonic crystal resonators. *Nano Lett.* **2010**, *10*, 99–104. [[CrossRef](#)]
12. Conteduca, D.; Brunetti, G.; Dell’Olio, F.; Armenise, M.N.; Krauss, T.F.; Ciminelli, C. Monitoring of individual bacteria using electro-phonic traps. *Biomed. Opt. Express* **2019**, *10*, 3463–3471. [[CrossRef](#)] [[PubMed](#)]
13. Lin, S.; Schonbrun, E.; Crozier, K. Optical manipulation with planar silicon microring resonators. *Nano Lett.* **2010**, *10*, 2408–2411. [[CrossRef](#)] [[PubMed](#)]
14. Cai, H.; Poon, A.W. Optical manipulation of microparticles using whispering-gallery modes in a silicon nitride microdisk resonator. *Opt. Lett.* **2011**, *36*, 4257–4259. [[CrossRef](#)] [[PubMed](#)]
15. Koya, A.N.; Cunha, J.; Guo, T.L.; Toma, A.; Garoli, D.; Wang, T.; Juodkazis, S.; Cojoc, D.; Proietti Zaccaria, R. Novel Plasmonic Nanocavities for Optical Trapping—Assisted Biosensing Applications. *Adv. Opt. Mat.* **2020**, *8*, 1901481. [[CrossRef](#)]
16. Conteduca, D.; Reardon, C.; Scullion, M.G.; Dell’Olio, F.; Armenise, M.N.; Krauss, T.F.; Ciminelli, C. Ultra-high Q/V hybrid cavity for strong light-matter interaction. *APL Phot.* **2017**, *2*, 086101. [[CrossRef](#)]
17. Dantham, V.R.; Holler, S.; Barbre, C.; Keng, D.; Kolchenko, V.; Arnold, S. Label-free detection of single protein using a nanoplasmonic-photonic hybrid microcavity. *Nano Lett.* **2013**, *13*, 3347–3351. [[CrossRef](#)]
18. Chen, Y.F.; Serey, X.; Sarkar, R.; Chen, P.; Erickson, D. Controlled photonic manipulation of proteins and other nanomaterials. *Nano Lett.* **2012**, *12*, 1633–1637. [[CrossRef](#)]
19. Lin, S.; Crozier, K.B. Trapping-assisted sensing of particles and proteins using on-chip optical microcavities. *ACS Nano* **2013**, *7*, 1725–1730. [[CrossRef](#)]
20. Conteduca, D.; Brunetti, G.; Pitruzzello, G.; Tragni, F.; Dholakia, K.; Krauss, T.F.; Ciminelli, C. Exploring the limit of multiplexed near-field optical trapping. *ACS Phot.* **2021**, *8*, 2060–2066. [[CrossRef](#)]
21. Kotnala, A.; DePaoli, D.; Gordon, R. Sensing nanoparticles using a double nanohole optical trap. *Lab A Chip* **2013**, *13*, 4142–4146. [[CrossRef](#)]
22. Yoo, D.; Gurunatha, K.L.; Choi, H.K.; Mohr, D.A.; Ertsgaard, C.T.; Gordon, R.; Oh, S.H. Low-power optical trapping of nanoparticles and proteins with resonant coaxial nanoaperture using 10 nm gap. *Nano Lett.* **2018**, *18*, 3637–3642. [[CrossRef](#)] [[PubMed](#)]
23. Kim, J.D.; Lee, Y.G. Trapping of a single DNA molecule using nanoplasmonic structures for biosensor applications. *Biomed. Opt. Exp.* **2014**, *5*, 2471–2480. [[CrossRef](#)] [[PubMed](#)]
24. Zhang, P.; Song, G.; Yu, L. Optical trapping of single quantum dots for cavity quantum electrodynamics. *Phot. Res.* **2018**, *6*, 182–185. [[CrossRef](#)]
25. Lu, Y.; Du, G.; Chen, F.; Yang, Q.; Bian, H.; Yong, J.; Hou, X. Tunable potential well for plasmonic trapping of metallic particles by bowtie nano-apertures. *Sci. Rep.* **2016**, *6*, 20594. [[CrossRef](#)] [[PubMed](#)]
26. Bendix, P.M.; Reihani, S.N.S.; Oddershede, L.B. Direct measurements of heating by electromagnetically trapped gold nanoparticles on supported lipid bilayers. *ACS Nano* **2010**, *4*, 2256–2262. [[CrossRef](#)] [[PubMed](#)]
27. Wang, K.; Schonbrun, E.; Steinvurzel, P.; Crozier, K.B. Trapping and rotating nanoparticles using a plasmonic nano-tweezer with an integrated heat sink. *Nat. Comm.* **2011**, *2*, 469. [[CrossRef](#)]
28. Xu, Z.; Song, W.; Crozier, K.B. Direct particle tracking observation and Brownian dynamics simulations of a single nanoparticle optically trapped by a plasmonic nanoaperture. *ACS Phot.* **2018**, *5*, 2850–2859. [[CrossRef](#)]
29. Xu, Z.; Song, W.; Crozier, K.B. Optical trapping of nanoparticles using all-silicon nanoantennas. *ACS Phot.* **2018**, *5*, 4993–5001. [[CrossRef](#)]
30. Yue, W.C.; Yao, P.J.; Xu, L.X.; Ming, H. All-dielectric bowtie waveguide with deep subwavelength mode confinement. *Front. Phys.* **2018**, *13*, 134207. [[CrossRef](#)]
31. Lu, Q.; Shu, F.J.; Zou, C.L. Dielectric bow-tie nanocavity. *Opt. Lett.* **2013**, *38*, 5311–5314. [[CrossRef](#)]

32. Zotev, P.G.; Wang, Y.; Sortino, L.; Severs Millard, T.; Mullin, N.; Conteduca, D.; Shagar, M.; Genco, A.; Hobbs, J.K.; Krauss, T.F.; et al. Transition Metal Dichalcogenide Dimer Nanoantennas for Tailored Light–Matter Interactions. *ACS Nano* **2022**, *16*, 6493–6505. [[CrossRef](#)] [[PubMed](#)]
33. Pesce, G.; Jones, P.H.; Maragò, O.M.; Volpe, G. Optical tweezers: Theory and practice. *Eur. Phys. J. Plus* **2020**, *135*, 949. [[CrossRef](#)]
34. Gan, Q.; Ding, Y.J.; Bartoli, F.J. “Rainbow” trapping and releasing at telecommunication wavelengths. *Phys. Rev. Lett.* **2009**, *102*, 056801. [[CrossRef](#)] [[PubMed](#)]
35. Hale, G.M.; Querry, M.R. Optical constants of water in the 200-nm to 200- $\mu$ m wavelength region. *Appl. Opt.* **1973**, *12*, 555–563. [[CrossRef](#)]
36. Malitson, I.H. Interspecimen comparison of the refractive index of fused silica. *J. Opt. Soc. Am.* **1965**, *55*, 1205–1209. [[CrossRef](#)]
37. Salzberg, C.D.; Villa, J.J. Infrared refractive indexes of silicon germanium and modified selenium glass. *JOSA* **1957**, *47*, 244–246. [[CrossRef](#)]
38. Dobrzynski, L.; Maradudin, A.A. Electrostatic edge modes in a dielectric wedge. *Phys. Rev. B* **1972**, *6*, 3810. [[CrossRef](#)]
39. Almeida, V.R.; Xu, Q.; Barrios, C.A.; Lipson, M. Guiding and confining light in void nanostructure. *Opt. Lett.* **2004**, *29*, 1209–1211. [[CrossRef](#)]
40. Fehr, A.R.; Perlman, S. Coronaviruses: An overview of their replication and pathogenesis. *Coronaviruses* **2015**, *1282*, 1–23.
41. Kingsbury, D.W. Paramyxoviridae. *Intervirology* **1978**, *10*, 137–152. [[CrossRef](#)]
42. Wang, S.; Shan, X.; Patel, U.; Huang, X.; Lu, J.; Li, J.; Tao, N. Label-free imaging, detection, and mass measurement of single viruses by surface plasmon resonance. *Proc. Natl. Acad. Sci. USA* **2010**, *107*, 16028–16032. [[CrossRef](#)] [[PubMed](#)]
43. Vollmer, F.; Arnold, S.; Keng, D. Single virus detection from the reactive shift of a whispering-gallery mode. *Proc. Natl. Acad. Sci. USA* **2008**, *105*, 20701–20704. [[CrossRef](#)] [[PubMed](#)]
44. Block, O.; Mitra, A.; Novotny, L.; Dykes, C. A rapid label-free method for quantitation of human immunodeficiency virus type-1 particles by nanospectroscopy. *J. Virol. Methods* **2012**, *182*, 70–75. [[CrossRef](#)] [[PubMed](#)]
45. Ciminelli, C.; Conteduca, D.; Dell’Olio, F.; Armenise, M.N. Design of an optical trapping device based on an ultra-high Q/V resonant structure. *IEEE Phot. J.* **2014**, *6*, 1–16. [[CrossRef](#)]
46. Serey, X.; Mandal, S.; Erickson, D. Comparison of silicon photonic crystal resonator designs for optical trapping of nanomaterials. *Nanotechnology* **2010**, *21*, 305202. [[CrossRef](#)]
47. Svoboda, K.; Block, S.M. Optical Trapping of Metallic Rayleigh Particles. *Opt. Lett.* **1994**, *19*, 930–932. [[CrossRef](#)]
48. Pelton, M.; Liu, M.; Kim, H.Y.; Smith, G.; Guyot-Sionnest, P.; Scherer, N.F. Optical trapping and alignment of single gold nanorods by using plasmon resonance. *Opt. Lett.* **2006**, *31*, 2075–2077. [[CrossRef](#)]
49. Yang, A.H.; Moore, S.D.; Schmidt, B.S.; Klug, M.; Lipson, M.; Erickson, D. Optical manipulation of nanoparticles and biomolecules in sub-wavelength slot waveguides. *Nature* **2009**, *457*, 71–75. [[CrossRef](#)]
50. Grigorenko, A.N.; Roberts, N.W.; Dickinson, M.R.; Zhang, Y. Nanometric optical tweezers based on nanostructured substrates. *Nat. Phot.* **2008**, *2*, 365–370. [[CrossRef](#)]
51. Bian, Y.; Zheng, Z.; Liu, Y.; Liu, J.; Zhu, J.; Zhou, T. Hybrid wedge plasmon polariton waveguide with good fabrication-error-tolerance for ultra-deep-subwavelength mode confinement. *Opt. Exp.* **2011**, *19*, 22417–22422. [[CrossRef](#)]